Identification of a new androgen receptor (AR) co-regulator BUD31 and related peptides to suppress wild-type and mutated AR-mediated prostate cancer growth *via* peptide screening and X-ray structure analysis

Cheng-Lung Hsu[1,2], **Jai-Shin Liu**[2,4], **Po-Long Wu**[4], **Hong-Hsiang Guan**[4,5], **Yuh-Ling Chen**[1,7], **An-Chi Lin**[2], **Huei-Ju Ting**[1], **See-Tong Pang**[3], **Shauh-Der Yeh**[1], **Wen-Lung Ma**[1,6], **Chung-Jung Chen**[4,5], **Wen-Guey Wu**[4,5,*], and **Chawnshang Chang**[1,6,*]

[1]The George Whipple Lab for Cancer Research, Departments of Pathology and Urology, University of Rochester Medical Center, Rochester, NY 14642

[2]Division of Hematology-Oncology, Chang Gung Memorial Hospital, Chang Gung University, Taoyuan 333, Taiwan

[3]Departments of Internal Medicine, Division of Urology, Department of Surgery, Chang Gung Memorial Hospital, Chang Gung University, Taoyuan 333, Taiwan

[4]National Synchrotron Radiation Center, Hsinchu 300, Taiwan

[5]Department of Physics and Institute of Bioinformatics and Structural Biology, National Tsing Hua University, Hsinchu 300, Taiwan

[6]Sex Hormone Research Center, China Medical University/Hospital, Taichung 104, Taiwan

[7]Institute of Oral Medicine, National Cheng Kung University, Tainan 701, Taiwan

Abstract

Treatment with individual anti-androgens is associated with the development of hot-spot mutations in the androgen receptor (AR), including T877A (hydroxyflutamide [HF]) and W741(C/L) (bicalutamide [CDX]). Here, we found that anti-androgens bound mt-ARs (HF-T877A-AR-LBD and CDX-W741L-AR-LBD) have similar binary structure to the 5α-dihydrotestosterone (DHT) bound wild type (wt) AR (DHT-wt-AR-LBD). Phage display revealed that these ARs bound to similar peptides, including BUD31, containing an Fxx(F/H/L/W/Y)Y motif cluster with Tyr in the +5 position. Structural analyses of the AR-LBD-BUD31 complex at 2.1 Å resolution revealed formation of an extra hydrogen bond between the Tyr+5 residue of the peptide and Gln733 of the AR AF2 domain, suggesting that peptides with Fxx(F/H/L/W/Y)Y

*Corresponding author: Chawnshang Chang, chang@urmc.rochester.edu and Wen-Guey Wu, wgwu@life.nthu.edu.tw.

motifs can interact with wt or mutated ARs. Functional studies showed that BUD31-related peptides suppressed transactivation of both DHT-wt-AR and HF-T877A-AR by interrupting AR N- and C-terminal interactions, thereby inhibiting wt and mutant AR-mediated prostate cancer cell growth. Collectively, these results suggest the combination of peptide screening and X-ray structure analysis as a new strategy for developing anti-androgens that simultaneously suppress both wt and mutated AR function.

Keywords

FxxLF; BUD31; crystallography; anti-androgen withdrawal syndrome; androgen receptor

1. Introduction

Anti-androgen withdrawal syndrome (AWS), initially described in the context of hydroxyflutamide (HF) treatment of prostate cancer as the response to withdrawal of therapy (Kelly and Scher, 1993), has since been documented for other anti-androgens, including bicalutamide (CDX), nilutamide, and chlormadinone (Akakura et al., 1998; Gomella et al., 1997; Small and Carroll, 1994). This syndrome has also been extended to steroid hormone withdrawal syndromes that occur with cessation of other steroid hormone treatments, including megestrol acetate (Dawson and McLeod, 1995), diethylstilbestrol (Bissada and Kaczmarek, 1995), and estramustine (Shibata et al., 1999). Approximately 30% of patients may experience this phenomenon, and withdrawing the anti-androgen treatment may have short-term benefits. The underlying mechanism is not clear, but mutation of the androgen receptor (AR) has frequently been reported. Some hot-spot mutations have been linked to treatment with individual anti-androgens, such as T877A, with hydroxyflutamide (HF) treatment, and W741(C/L), with bicalutamide (CDX) treatment (Hara et al., 2003). The ligand specificity of T877A AR is lost; thus, this receptor can be activated by both androgens and anti-androgens (Miyamoto et al., 2004).

The AR is a ligand-activated transcription factor that belongs to the nuclear receptor superfamily (Chang et al., 1988; Lubahn et al., 1988). The transcriptional activity of the AR is modulated by co-regulators such as ARA70, also known as NCOA4 (nuclear receptor coactivator 4) and SHP, also known as NR0B2 (nuclear receptor subfamily 0, group B, member 2) (Heinlein and Chang, 2002). The AR and other nuclear receptors can bind to the canonical LxxLL motif in these co-regulators (Darimont et al., 1998; Jouravel et al., 2007), with the AR preferring aromatic-rich FxxLF-like motifs. Studies of the first (+1) and the fifth (+5) amino acid positions of the FxxLF motif indicate that these residues are involved in mediating high affinity and specific interactions with the AR ligand-binding domain (LBD) (Dubbink et al., 2006). Furthermore, interchanging F and Y at the +5 position, as in FxxLF, FxxLY and FxxFF, modulates coregulator binding activity (He et al., 2000; Hsu et al., 2003; van de Wijngaart et al., 2006). In fact, the FxxLF-like motif exists in many AR coregulators and plays an important role in modulating coregulator-mediated AR functions (Heinlein and Chang, 2002; Hsu et al., 2003; Yeh and Chang, 1996). This FxxLF-like motif is also found in the AR N-terminus and is pivotal in mediating the interaction of AR N- and C-termini, which is required for full AR function (He et al., 2000; He et al., 2002).

Upon androgen binding to the AR, helix 12 undergoes a conformational change that allows opening of the AF2 (activation function 2) hydrophobic cleft formed by helices 3, 4, 5, and 12 of the LBD to accommodate the bulky peptide side chains. Specifically, the FxxLF peptide forms a short α-helix with Phe+1, Leu+4, and Phe+5 that binds hydrophobic face down in the L-shaped AF2 cleft of the AR. Electrostatic interactions involving Lys720 and Glu897 at either end of the AF2 cleft interact with the backbone carbonyl group of Phe+5 and the amine group of residue +1 or -1, respectively (Dubbink et al., 2004; Hur et al., 2004). The side chains of two key amino acid residues, Met734 and Met894, also help to form the hydrophobic binding pocket for the +1 and +5 position of the motif. In contrast, Leu+4 binds to a shallow, hydrophobic patch in the sidewall of the L-shaped groove and is largely solvent exposed. The other intra-motif and flanking amino acids support the interaction of the peptide with the AR (Hur et al., 2004).

Using 5α-dihydrotestosterone (DHT) wild-type AR-DBD-LBD (wt-AR-DBD-LBD) and HF mutant T877A AR-DBD-LBD (HF-T877A-AR-DBD-LBD) as baits, we found that screened peptides were enriched for Tyr+5. Further characterization of the roles of the peptide motifs using both functional and structural approaches led us to conclude that the newly identified BUD31 peptide motif functions to suppress both DHT-mediated AR and HF-mediated T877A-AR transactivation, thus potentially offering a better therapeutic approach for suppressing prostate cancer in patients with AWS.

2. Materials and methods

2.1. Materials and plasmids

DHT and CDX were obtained from Sigma Chemical Co. (St. Louis, MO) and HF was obtained from Schering-Plough (Kenilworth, NH). The Ph.D.-12 peptide library was purchased from New England Biolabs (Beverly, MA). The human prostate cancer cell lines, PC-3 and LNCaP, were purchased from the American Type Culture Collection (Manassas, VA). The AR expression plasmids PCMV-Flag-AR and pCMX-VP16-AR were constructed as described previously (Nishimura et al., 2003; Yeh and Chang, 1996). BUD31 cDNA, prepared from human LNCaP cells, was cloned into the p3xFLAG-CMV vector (Sigma Chemical Co.). Motif-mutants of the BUD31 plasmid, p3X-FLAG-mt-AxxAA, were generated by site-directed mutagenesis using a kit obtained from Stratagene (La Jolla, CA). Peptides with the following sequences were synthesized by Genesis Biotech Inc. (Hsintien, Taiwan): Biotin-BUD31p, Biotin-KTRYI-FDLFY-KRKAY; Biotin-3-18, Biotin-NTNA-FSRLF-YPS; Biotin-C320, Biotin-SDSA-FSRLY-TRS; Transactivator of Transcription (TAT), fluorescein-GGGYGRKKRRQRRRG; TAT-BUD31p, fluorescein-TAT-KTRYI-FDLFY-KRKAY; TAT-3-18, fluorescein-TAT-NTNA-FSRLF-YPS; TAT-C320, TAT-SDSA-FSRLY-TRS; and TAT-3-14, fluorescein-TAT-DHSK-LYSLL-QSS. All peptides were dissolved in water. Anti-AR (C19) and anti-BUD31 antibodies were purchased from Santa Cruz Biotechnology (Santa Cruz, CA) and Sigma-Aldrich, respectively.

2.2. Co-immunoprecipitation

The co-immunoprecipitation (Co-IP) procedure has been previously described in detail (Shyr et al., 2010). Here, LNCaP cells were transfected with 5 mg of p3xFLAG-BUD31 and

harvested after 48 h, and nuclear extracts were prepared for Co-IP assays. A 400-μl aliquot of each extract was first incubated with anti-Flag or anti-AR (C19) antibody (Santa Cruz Biotechnology) overnight at 4°C, and then with Protein G Sepharose for an additional 16 h at 4°C. Protein G Sepharose containing the immune complex was then washed three times with washing buffer (50 mM Tris–HCl pH 7.4, 100 mM NaCl, 5 mM $CaCl_2$, 5 mM $MgCl_2$, 0.1% Nonidet P-40) and resuspended in sodium dodecyl sulfate (SDS)-containing sample buffer. Flag- and AR-associated complexes were immunoprecipitated with anti-Flag and anti-AR antibodies, respectively. The isolated protein complexes were fractionated, transferred to membranes, and immunoblotted with anti-AR or anti-BUD31 antibodies.

2.3. Patient enrollment

Primary prostate tumors were collected from patients undergoing a prostate tumor biopsy from 2007 to 2009. Written informed consent was obtained from all patients prior to surgery. The studies were approved by the Institutional Review Board of Chang Gung Memorial Hospital, Taoyuan, Taiwan.

2.4. Cloning, expression, and purification of human AR proteins and phage-display procedure

AR-DBD-LBD cDNA (amino acids 548–919) and AR-LBD cDNA (amino acids 663–919) were amplified from the AR expression vector pSG5-AR by polymerase chain reaction (PCR) and inserted into the pET28c vector (Novagen, San Diego, CA). The pET28c-T877A-AR-DBD-LBD vector was generated using the Stratagene site-directed mutagenesis kit. Protein expression and purification, and phage-display procedures were described previously (Chang et al., 2005; Hsu et al., 2003; Hur et al., 2004).

2.5. Crystallization, data collection, and structural determination

AR-LBD proteins were crystallized with the hanging-drop method using a commercial kit. After extensive trials, individual crystals of the AR-LBD protein were obtained after 2 d in a solution of 1.6 M magnesium sulfate heptahydrate in 0.1 mM MES buffer (pH 6.5), reaching a maximal size within 2 wk. Rhombus-shaped AR-LBD protein crystals ($0.6 \times 0.6 \times 2.5$ mm) were transferred to solutions containing different 3-6-fold molar excess peptides and incubated for 1 h at room temperature. Finally, crystals were soaked in a protectant containing mother liquid and an additional 20% (v/v) glycerol for 20 s and placed in the cold stream at 100K.

Data were collected using an ADSC Quantum 315r CCD detector at the BL13B at the National Synchrotron Radiation Research Center (NSRRC) in Hsinchu, Taiwan. The datasets were indexed and integrated using HKL2000 and SCALEPACK software (Z. Otwinowski and W. Minor, 1997). The structures were determined by the molecular replacement method with the AMore program using the AR-LBD ternary structure (PDB code: 1T73) as the search model (Navaza, 1994). Models were built with the Coot program (Emsley and Cowtan, 2004). Refinement was carried out with the REFMAC 5 program (Murshudov et al., 1997). Water molecules were added and checked using the ARP/WARP program (Perrakis et al., 1999). The refined model was checked using the PROCHECK program (Laskowski et al., 1993). Protein structural figures were prepared with the PyMOL

program (Schrodinger, 2010). The coordinates have been deposited in the Protein Data Bank. Data collection and statistics are summarized in Supplementary Table 1.

2.6. Surface plasmon resonance

Synthetic biotinylated peptides were injected onto a streptavidin-immobilized chip and allowed to bind; binding was detected in resonance units (400 resonance units for peptides only). Different concentrations (12–48 nM) of AR-DBD-LBD in an HBS-P buffer (10 mM HEPES pH 7.4, 0.15 M NaCl, 0.05% surfactant P20) containing 10 nM DHT or 10 μM HF were injected at a flow rate of 30 μl/min, and binding to peptides, in resonance units, was measured. A blank flow cell served as the negative control, and background signals were subtracted from sample signals. Sensorgrams of association and dissociation were recorded and analyzed using BIAevaluation software 3.0 (Biacore AB, Uppsala, Sweden). A simple 1:1 Langmuir model was employed to fit the data. A two-state conformational change model was used, as previously described (Warnmark et al., 2002).

2.7. Glutathione Sepharose transferase (GST) pull-down assay

Wild-type (wt) and mutant (mt) GST-BUD31 and GST control proteins were purified as described by the manufacturer of the GST pull-down assay (Amersham Biosciences, Sunnyvale, CA). Five microliters of *in vitro*-translated [^{35}S] methionine-labeled AR (full-length, N-terminus, or C-terminus) was incubated with wt or mt GST-BUD31 protein or GST control bound to glutathione-Sepharose beads in the presence or absence of 10 nM DHT (Hsu et al., 2003). After extensive washing, the pull-down complex was loaded onto an 8% or 10% polyacrylamide gel and visualized by autoradiography. The input represented 20% of the amount of labeled protein used in the pull-down assay.

2.8. Mammalian two-hybrid assay, transfection, and reporter gene assay

Procedures were performed as previously described in detail (Hsu et al., 2003). The PC-3 cell line was used in mammalian two-hybrid assays and reporter gene assays.

2.9. ChIP assay

LNCaP cells were grown in phenol-red-free RPMI-1640 medium supplemented with 10% FBS. LNCaP cells were transfected with P3xFlag-BUD31 plasmid using the Superfect reagent (Qiagen, Valencia, CA), as described by the manufacturer. After transfection, the cells were cultured overnight in phenol-red-free RPMI-1640 supplemented with 8% charcoal-dextran–stripped FBS. Cells were treated with or without 10 nM DHT for 2 h before cross-linking for 10 min with a final concentration of 1% formaldehyde in growth media. Cells were washed twice with ice-cold PBS and pelleted. Chromatin immunoprecipitation (ChIP) assays were performed using a Magna ChIP kit (Millipore, Billerica, MA). Antibodies used in these experiments were anti-AR (PG-21; Millipore), anti-BUD31 (H-61; Santa Cruz Biotechnology), anti-Flag M2 (Sigma), and anti-RNA polymerase II (clone CTD4H8; Millipore). Two microliters of DNA extract (out of a total of 50 μl) was used in each PCR. The primer pairs used were as follows: ARE I/II (-459 to -121), 5′-GCC AAG ACA TCT ATT TCA GGA GC-3′ (forward) and 5′-CCC ACA CCC AGA GCT GTG GAA GG-3′ (reverse); and ARE III (-4288 to -3922), 5′-GGG GTT TGT

GCC ACT GGT GAG-3′ (forward) and 5′-GGG AGG CAA TTC TCC ATG GTT-3′ (reverse) (Shatkina et al., 2003).

2.10. Cell growth assay

LNCaP cells were grown in RPMI medium containing 10% FBS. Cells were plated at 5×10^4 cells/well in 24-well plates and incubated with or without 0.2 nM DHT and 10 μM peptide for 2 to 7 d. Cell growth was assessed using the MTT (3-{4,5-dimethylthiazol-2-yl}-2,5-diphenyltetrazolium bromide) assay (Hsu et al., 2005). At each time point, 50 μl of a 5-mg/ml MTT solution was added to each well containing 500 μl of medium and incubated for 3 h; 500 μl of isopropyl alcohol was added to dissolve the reduced formazan product. The absorbance of each well was measured at a wavelength of 590 nm in a DU 640B spectrophotometer (Beckman, Fullerton, CA) according to the manufacturer's protocol. Values presented in figures are mean $OD_{590} \pm SD$ from at least three independent reaction wells.

2.11. Statistical analysis

Data are presented as means ± SEM. Differences between two groups were assessed using the unpaired two-tailed Student's *t* test.

3. Results and Discussion

3.1. Binding profiles of binary liganded–AR-LBD complex structures

AWS, in which anti-androgens become agonists, is found in anti-androgen-treated prostate cancer patients, who are frequently found to harbor the mutated T877A-AR (with HF treatment) or mutated W741L-AR (with CDX treatment) (Kelly et al., 1997; Miyamoto et al., 2004). These findings suggest that liganded wt and mutant ARs (DHT-wt-AR, HF-T877A-AR, and CDX-W741L-AR) might share similar structures that could recognize common AR-associated peptide motifs. Therefore, structures of AR-LBD co-crystals with androgen or anti-androgen might reveal structural variations among these mutants.

Three binary complex structures were obtained: DHT-wt-AR-LBD, HF-T877A-AR-LBD, and CDX-W741L-AR-LBD. All the crystallographic parameters of these crystals belonged to the orthorhombic group with one molecule per asymmetric unit, results similar to those observed previously (Hur et al., 2004). Furthermore, all models were refined to R and free-R values that conformed to a typical range. Crystallographic statistics are summarized in Supplemental Table 1.

To further verify the structural-rearrangement effects trigged by androgen versus anti-androgens, we overlapped these binary structures. The equivalent Cα atoms were identical (root mean square deviation [RMSD] < 0.5 Å) among these structures, indicating that these compounds propelled identical structural rearrangements of the AR architecture (Fig. 1A). In addition to the overall structures, the binding sites of the androgens were also compared. DHT bound to four surrounding residues (Asn705, Gln711, Arg752, and Thr877) of the AR protein by forming hydrogen bonds. Binding contacts were similar for HF-T877A and CDX-W741L AR mutants, except that the contact involving Thr877 was lacking in the HF-T877A

mutant and the CDX-W741L mutant formed an additional hydrogen bond with the O atom of Leu704 (Fig. 1B).

3.2. Tyrosine in the +5 position of the peptide motif is enriched in peptides that associate with DHT-wt-AR-DBD-LBD and HF-T877A-AR-DBD-LBD

To test if these liganded-AR complexes, which share a similar structure, recognize similar peptide motifs, we used bacterially expressed DHT-wt-AR-DBD-LBD and HF-T877A-AR-DBD-LBD proteins as baits to screen potential peptides using phage display. We found that peptides containing a tyrosine in the +5 position of the motif, including those with the sequence FxxLY, FxxFY, FxxHY, FxxWY and FxxYY, were frequently identified in the screened peptides (Table 1). We then used a mammalian two-hybrid assay to confirm the interaction of these screened peptides with full-length DHT-wt-AR or HF-T877A-AR and found that they were able to interact with the ARs. Some peptides screened using the HF-T877A protein as bait, such as those with an FxxFY motif (A41, B37, and B45) or FxxHY motif (and HF-26), showed a tendency to interact more strongly with HF-T877A-AR than with DHT-T877A-AR in these assays (Table 1).

3.3. Peptide motif complex structures

Although the binary architectures of the AR variants were similar to those of the wt-AR, the affinity between peptides and AR protein varied. To clarify how peptides preferentially interact with these proteins, we determined the ternary complex structures of the AR proteins in the presence of various peptides. As expected, an additional density map on the surface was found for each and was modeled to a short α-helical peptide given by the indicated sequences. These peptides were coordinated by residues L720 and E894, suggesting that these peptides bound to the AF2 sites formed by helices 3 (H3), 5 (H5), and 12 (H12) (Hur et al., 2004).

Seventeen ternary complex structures were determined and divided into three groups: wt-AR, T877A-AR, and W741L-AR. To gain further insight into the structural consequences of peptide association, we overlapped the binary (absence of peptides) and ternary (presence of peptides) structures. Superpositions of the equivalent Cα atoms were identical (RMSD < 0.5 Å) among ternary wt-AR structures, indicating that these structures share identical folds owing to DHT binding. Moreover, association of the peptides did not influence the architecture of the wt-AR. Similar results were obtained with respect to the ternary complex structures of AR variants. To further confirm these structural similarities, we assessed differences between wt-AR and variants by overlapping the ternary wt-AR-FQNLF structure with that of T877A-AR-FQNLF and W741L-AR-FQNLF structures. RMSD values of 1.0 and 0.3 Å in the Cα backbone were observed for T877A-AR-FQNLF and W741L-AR-FQNLF structures, respectively, with respect to that of wt-AR-FQNLF, indicating that the folding of the overall structures is identical. These findings indicate that the structural rearrangements induced in mutant ARs by HF and CDX treatment are similar. Collectively, these results indicate that the similarity of the rearrangements that occur with AWS carries significant implications.

Although the peptides were unable to disturb the scaffolds of the ARs, the resolved structures revealed slight differences in the interactions between peptides and the AF2 site, such as accommodations in the +1 and +5 positions of the peptide. In the front-end position (+1) of the AF2 site, the mobile $O\delta2$ atoms of residue E897 make variable hydrogen bond contacts with the N atoms of peptides at -1 or -2 positions. These contacts not only provide the major stabilizing influence, they also contribute to the variable affinities of peptides for protein (Fig. 2A). Notably, residues M734 and M897 on either side of the +1 position provide the structural flexibility necessary to accommodate the +1 peptide position van der Waals interactions.

The back-end interactions are remarkably distinct from those of the front-end area. The hydrogen bond contacts in this area are redistributed after association of the peptides. In the absence of the peptide, the H3 and H5 helices are stabilized by a hydrogen bond with the $N\varepsilon$ atom of Lys720 and the $O\delta2$ atom of Q733 of the protein (Fig. 2B, AR). However, association of the peptides disrupts these stabilizing interactions in two ways. First, in the presence of the peptide, the N atoms at Lys720 turn toward to the O atoms of the +5 peptide residue, with which it forms a hydrogen bond, providing a new constraining bond between the peptide and the protein (Fig. 2B, AR-FQNLF). Second, with the change in the +5 peptide position to Tyr, the side chain of the Q733 residue flips the $N\varepsilon$ atom over to face the hydroxyl group of the peptide (Fig. 2B, AR-FxxxY), enabling a hydrogen bond to form between the nitrogen atom and the hydroxyl group. This result indicates that Tyr in the +5 position of the peptide provides an extra constraining force through formation of a hydrogen bond interaction, which also enhances the association between peptide and protein.

Previous structural studies have demonstrated that ARs can accommodate short peptides through their conserved residues K720, M734, M894, and E897 (Hur et al., 2004). To examine this in the context of our resolved structures, we superposed the peptides and compared their arrangements within this binding pocket. These peptides bound to the wt-AR protein overlapped well, exhibiting virtually identical positions of $C\alpha$ atoms (Fig. 3A); similar results were obtained for binding to T877A-AR and W741L-AR (Fig. 3B and C). In addition to interactions at both ends of the peptides, the +4 position of the groove is suitable for accommodating bulky side chains of residues (Dubbink et al., 2004). Our resolved complex structures also demonstrated that bulky side chains of the +4 residue in the peptide adopt a *trans* conformation that extends into the groove. Moreover, peptides with aromatic bulky side chains in the +4 residue showed greater affinity for protein than peptides containing other hydrophobic residues (Table 2). The bulky side chain of +4 residues, including Trp and His, were exposed toward the broad groove. No hydrogen bond contacts were made between the side chain of the +4 peptide and the protein, whereas the orientation of this side chain was influenced by the surrounding hydrophobic residues, V713, V716 and K717. Therefore, the surrounding hydrophobic environment promotes a favorable orientation of the side chain in this groove. Remarkably, the side chains of residues in the +2 and +3 positions were superposed well and did not interact with the protein (Fig. 3D).

Previous phage-display screens indicated that the +4 position of peptides favored hydrophobic amino acids (Leu and Phe), whereas the +5 position favored aromatic amino acids (Phe and Tyr). Using surface plasmon resonance to determinate the kinetic constants

for the association between the interacting molecules, we confirmed that the variant peptides are capable of associating with AR protein. However, the K_d (M) values obtained from sensorgrams were remarkably different in –HY peptides (Table 2). A comparison of the results reported for variant peptides indicated that the -HY peptide associated faster with AR proteins than others peptides, indicating that the hydrophobicity of the side chain of the +4 residue influences binding affinity. These results, taken together with the major role of variations in electromagnetic forces in both ends in the overall attraction, suggest that the hydrophobic side chain modulates the affinity of peptides for proteins through contributions to intermolecular force and steric hindrance.

3.4. BUD31, containing an FxxFY motif, is a new AR co-regulator

A computer search of existing protein databases found an 18-kD protein, BUD31 (also known as EDG-2/hG10) containing the FxxFY motif ([61]FDLFY[65]). Early studies detected BUD31 in human umbilical vein endothelial cells (Hla et al., 1995) and showed that it shared 93% homology with G10 from the African frog *Xenopus*. In yeast, BUD31 is involved in spliceosome assembly and promotes pre-mRNA splicing (Saha et al., 2012). However, little is known about the role of BUD31 in humans. Therefore, we chose BUD31 and its FxxFY motif for further study.

In Co-IP assays using anti-AR or anti-Flag antibodies to pull down AR-BUD31 protein complexes in LNCaP cells expressing 3×-Flag-BUD31 (Fig. 4A), we found that wt-BUD31 with the FxxFY motif interacted with the GST-AR, whereas mt BUD31 with an AxxAA motif did not (Fig. 4B). These data suggest that BUD31 does indeed interact with the AR via its FxxFY motif. We also found that BUD31 interacted with the AR N-terminus (Fig. 4B). We then demonstrated that, in AR-negative PC-3 prostate cancer cells co-transfected with AR and an AR-responsive MMTV-LUC reporter construct, treatment with 10 nM DHT resulted in AR transactivation (Fig. 4C). Moreover, exogenous overexpression of BUD31-wt-FxxFY further enhanced AR transactivation in a dose-dependent manner (Fig. 4C). In contrast, expression of mutant BUD31 with an AxxAA motif had little effect on AR transactivation.

We further applied ChIP assays to determine whether BUD31 bound to endogenous ARs at promoter regions of target genes. ARs and BUD31 were constitutively associated with ARE I/II and were recruited to ARE III in a DHT-dependent manner (Fig. 4D). Importantly, we found that full-length BUD31 suppressed interactions of AR N- and C-termini (Fig. 4E). Finally, immunohistochemical staining revealed that both the AR and BUD31 were present in epithelial and stromal cells of benign prostatic hyperplasia tissue (Fig. 4F), suggesting the coexistence of the AR and the BUD31 peptide in the human prostate.

Taken together, the results shown in Figure 4A-F demonstrate that BUD31, containing an FxxFY motif, is a bona fide AR co-activator that enhances AR transactivation in prostate cells.

3.5. The BUD31-FxxFY peptide effectively suppresses DHT-AR-mediated cell growth

The above data suggest that the short peptide BUD31 could bind tightly to AR-LBD and AR-DBD-LBD; therefore, we were interested in testing whether binding of this or other FxxFY motif-like peptides to the AR modulated AR transactivation. As expected, BUD31 and other AR-DBD-LBD-related peptides (see sequences in Fig. 5A) suppressed AR transactivation in the presence of DHT and HF (Fig. 5B).

We then examined the potential pathophysiological consequences of suppression of AR transactivation by BUD31-related peptides by conjugating these peptides to the leading TAT sequence (which facilitates import of conjugated peptides into the cytosol) and transducing them into LNCaP cells. The results showed that BUD31 and related peptides suppressed LNCaP cell growth, with the BUD31 peptide exhibiting the greatest inhibitory effect (Fig. 5C). Using an MMTV-LUC reporter assay, we found that the BUD31 peptide suppressed AR N-C interactions in a dose-dependent manner, suggesting a potential molecular mechanism by which BUD31 peptide-AR interactions suppress AR transactivation (Fig. 5D).

4. Conclusions

As a unique pathological feature of cancer, AWS could be a target for the development of new anti-cancer treatment strategies. Here, we compared the binary structures of wild-type and its variants, and demonstrated that anti-androgen-mt-AR complexes share a folding similar to that of DHT-wt-AR. This phenomenon explained the facile transition between androgen antagonist and agonist in this disease. Our ligand-AR-peptide ternary structure analysis revealed that the equivalent Cα atoms were almost identical, with RMSD values < 0.5 Å within these structures, indicating that each altered AF2 site is very similar. The AF2 sites among these mt-ARs were found to be fully functional, and therefore capable of recruiting identical peptide motifs as well as those in wt-AR.

Among these AF2 sites, however, we observed different electrostatic interactions between the peptides and proteins. One charge clump residue, Glu897, was found to make HB contacts with the -1 or -2 positions of the peptides; this was due to the polar character of its side chain, and demonstrated an alternative means for connecting a peptide to the protein (Hur et al., 2004). In contrast, the 5th position of AR-interacting peptides was generally tyrosine rich, and replacement of Phe with Tyr at this position obviously enhanced the peptide-protein interaction, resulting in the formation of an additional HB between the hydroxyl of the 5th residue of the peptide and the Q733 residue of AR (Fig. 2B). Both interactions strain the peptide and significantly enhanced the binding affinity.

Aside of the both ends of AF2 pocket, both the Val713 residue and its neighboring hydrophobic residues (e.g., Leu712 and Val716) may provide attractions to the side chain of the 4th residue of the AR-interacting peptide. The side chains of these residues were found to have higher variety compared to the first and the 5th residue of the peptides as shown in Figures 2 and 3. Furthermore, the kinetic parameters of the peptide-protein interaction may be influenced by the selectivity of this AF2 groove. For example, the presence of a histidine residue, with a characteristic hydrophilic motif in its side chain, in AR-interacting peptides

significantly decreased the ability of the peptide and protein to interact. This distinctive affinity suggested that the sequence preference for the associating peptide arose at least partially from the side chain of the 4th residue.

In addition to competition for ligand binding with the AR-LBD, the AR-targeting mechanism was found to involve the abrogation of AR N-C and AR-coregulator interactions, which use the same AR cofactor-binding groove (He et al., 2002; Trapman and Dubbink, 2007). The AR antagonist, EPI-001 (Andersen et al., 2010), the protein, MAGE-11 (melanoma antigen family A) (Bai et al., 2005), the AR N-terminus itself (Quayle et al., 2007; Watson et al., 2010), the AR-degrading chemical, ASC-J9 (Yang et al., 2007), and AR-LBD BF-3-blocking small molecules (Estebanez-Perpina et al., 2007) have all been shown to disrupt AR-related functions by interfering with AR N-C interactions and/or AR co-regulator functions. However, some peptides and small molecules have been shown to suppress the AR-mediated transcription and growth of prostate cells by directly targeting the AR cofactor-binding groove (Axerio-Cilies et al., 2011; Hsu et al., 2005; van de Wijngaart et al., 2011). Here, we showed that the FxxFY-containing BUD31 peptide can block AR transcriptional activity, the AR N-C interaction, and AR-mediated cancer cell growth.

Using a unique approach that combined phage-display screening and X-ray crystal structure analysis of the AR cofactor-binding groove, we developed a new strategy for identifying anti-AR drugs containing an FxxFY motif, and used this strategy to identify the AR co-activator, BUD31, which was found to interact tightly with the AR. Recent studies have provided proof of principle for the notion that a peptidomimetic molecule can block AR-related functions by disrupting peptide/cofactor-AR interactions (Gunther et al., 2009; Hsu et al., 2014; Levine et al., 2012; Ravindranathan et al., 2013). Excellent studies have shown that the LxxLL-mimetic small molecule, D2, can block AR nuclear translocation, the AR-cofactor interaction and AR-mediated cell growth, and may potentially influence the functions of other steroid hormone receptors (Ravindranathan et al., 2013). The above-described peptidomimetic molecules sterically hinder the critical protein-protein interactions of AR, but do not suffer the same limitations as peptide therapeutics (e.g., facile degradation by peptidases, poor tissue penetration and lower target specificity). Our present data and the previous findings should pave the way for the future design of highly specific and efficient AR-targeting small molecules.

Supplementary Material

Refer to Web version on PubMed Central for supplementary material.

Acknowledgments

References

Akakura K, Akimoto S, Furuya Y, Ito H. Incidence and characteristics of antiandrogen withdrawal syndrome in prostate cancer after treatment with chlormadinone acetate. Eur Urol. 1998; 33:567–571. [PubMed: 9743699]

Andersen RJ, Mawji NR, Wang J, Wang G, Haile S, Myung JK, Watt K, Tam T, Yang YC, Banuelos CA, Williams DE, McEwan IJ, Wang Y, Sadar MD. Regression of castrate-recurrent prostate cancer by a small-molecule inhibitor of the amino-terminus domain of the androgen receptor. Cancer Cell. 2010; 17:535–546. [PubMed: 20541699]

Axerio-Cilies P, Lack NA, Nayana MR, Chan KH, Yeung A, Leblanc E, Guns ES, Rennie PS, Cherkasov A. Inhibitors of androgen receptor activation function-2 (AF2) site identified through virtual screening. J Med Chem. 2011; 54:6197–6205. [PubMed: 21846139]

Bai S, He B, Wilson EM. Melanoma antigen gene protein MAGE-11 regulates androgen receptor function by modulating the interdomain interaction. Mol Cell Biol. 2005; 25:1238–1257. [PubMed: 15684378]

Bissada NK, Kaczmarek AT. Complete remission of hormone refractory adenocarcinoma of the prostate in response to withdrawal of diethylstilbestrol. J Urol. 1995; 153:1944–1945. [PubMed: 7752364]

Chang CS, Kokontis J, Liao ST. Molecular cloning of human and rat complementary DNA encoding androgen receptors. Science. 1988; 240:324–326. [PubMed: 3353726]

Chang CY, Abdo J, Hartney T, McDonnell DP. Development of peptide antagonists for the androgen receptor using combinatorial peptide phage display. Mol Endocrinol. 2005; 19:2478–2490. [PubMed: 16051662]

Darimont BD, Wagner RL, Apriletti JW, Stallcup MR, Kushner PJ, Baxter JD, Fletterick RJ, Yamamoto KR. Structure and specificity of nuclear receptor-coactivator interactions. Genes Dev. 1998; 12:3343–3356. [PubMed: 9808622]

Dawson NA, McLeod DG. Dramatic prostate specific antigen decrease in response to discontinuation of megestrol acetate in advanced prostate cancer: expansion of the antiandrogen withdrawal syndrome. J Urol. 1995; 153:1946–1947. [PubMed: 7538601]

Dubbink HJ, Hersmus R, Pike AC, Molier M, Brinkmann AO, Jenster G, Trapman J. Androgen receptor ligand-binding domain interaction and nuclear receptor specificity of FXXLF and LXXLL motifs as determined by L/F swapping. Mol Endocrinol. 2006; 20:1742–1755. [PubMed: 16627595]

Dubbink HJ, Hersmus R, Verma CS, van der Korput HA, Berrevoets CA, van Tol J, Ziel-van der Made AC, Brinkmann AO, Pike AC, Trapman J. Distinct recognition modes of FXXLF and LXXLL motifs by the androgen receptor. Mol Endocrinol. 2004; 18:2132–2150. [PubMed: 15178743]

Emsley P, Cowtan K. Coot: model-building tools for molecular graphics. Acta crystallographica. 2004; 60:2126–2132.

Estebanez-Perpina E, Arnold LA, Nguyen P, Rodrigues ED, Mar E, Bateman R, Pallai P, Shokat KM, Baxter JD, Guy RK, Webb P, Fletterick RJ. A surface on the androgen receptor that allosterically regulates coactivator binding. Proc Natl Acad Sci U S A. 2007; 104:16074–16079. [PubMed: 17911242]

Gomella LG, Ismail M, Nathan FE. Antiandrogen withdrawal syndrome with nilutamide. J Urol. 1997; 157:1366. [PubMed: 9120950]

Gunther JR, Parent AA, Katzenellenbogen JA. Alternative inhibition of androgen receptor signaling: peptidomimetic pyrimidines as direct androgen receptor/coactivator disruptors. ACS Chem Biol. 2009; 4:435–440. [PubMed: 19441848]

Hara T, Miyazaki J, Araki H, Yamaoka M, Kanzaki N, Kusaka M, Miyamoto M. Novel mutations of androgen receptor: a possible mechanism of bicalutamide withdrawal syndrome. Cancer Res. 2003; 63:149–153. [PubMed: 12517791]

He B, Kemppainen JA, Wilson EM. FXXLF and WXXLF sequences mediate the NH2-terminal interaction with the ligand binding domain of the androgen receptor. J Biol Chem. 2000; 275:22986–22994. [PubMed: 10816582]

He B, Minges JT, Lee LW, Wilson EM. The FXXLF motif mediates androgen receptor-specific interactions with coregulators. J Biol Chem. 2002; 277:10226–10235. [PubMed: 11779876]

Heinlein CA, Chang C. Androgen receptor (AR) coregulators: an overview. Endocr Rev. 2002; 23:175–200. [PubMed: 11943742]

Hla T, Jackson AQ, Appleby SB, Maciag T. Characterization of edg-2, a human homologue of the Xenopus maternal transcript G10 from endothelial cells. Biochim Biophys Acta. 1995; 1260:227–229. [PubMed: 7841202]

Hsu CL, Chen YL, Ting HJ, Lin WJ, Yang Z, Zhang Y, Wang L, Wu CT, Chang HC, Yeh S, Pimplikar SW, Chang C. Androgen receptor (AR) NH2- and COOH-terminal interactions result in the differential influences on the AR-mediated transactivation and cell growth. Mol Endocrinol. 2005; 19:350–361. [PubMed: 15514032]

Hsu CL, Chen YL, Yeh S, Ting HJ, Hu YC, Lin H, Wang X, Chang C. The use of phage display technique for the isolation of androgen receptor interacting peptides with (F/W)XXL(F/W) and FXXLY new signature motifs. J Biol Chem. 2003; 278:23691–23698. [PubMed: 12714604]

Hsu CL, Liu JS, Lin AC, Yang CH, Chung WH, Wu WG. Minoxidil may suppress androgen receptor-related functions. Oncotarget. 2014; 5:2187–2197. [PubMed: 24742982]

Hur E, Pfaff SJ, Payne ES, Gron H, Buehrer BM, Fletterick RJ. Recognition and accommodation at the androgen receptor coactivator binding interface. PLoS Biol. 2004; 2:E274. [PubMed: 15328534]

Jouravel N, Sablin E, Arnold LA, Guy RK, Fletterick RJ. Interaction between the androgen receptor and a segment of its corepressor SHP. Acta Crystallogr D Biol Crystallogr. 2007; 63:1198–1200. [PubMed: 18007036]

Kelly WK, Scher HI. Prostate specific antigen decline after antiandrogen withdrawal: the flutamide withdrawal syndrome. J Urol. 1993; 149:607–609. [PubMed: 7679759]

Kelly WK, Slovin S, Scher HI. Steroid hormone withdrawal syndromes. Pathophysiology and clinical significance. Urol Clin North Am. 1997; 24:421–431. [PubMed: 9126240]

Laskowski RA, Moss DS, Thornton JM. Main-chain bond lengths and bond angles in protein structures. J Mol Biol. 1993; 231:1049–1067. [PubMed: 8515464]

Levine PM, Imberg K, Garabedian MJ, Kirshenbaum K. Multivalent peptidomimetic conjugates: a versatile platform for modulating androgen receptor activity. J Am Chem Soc. 2012; 134:6912–6915. [PubMed: 22509763]

Lubahn DB, Joseph DR, Sullivan PM, Willard HF, French FS, Wilson EM. Cloning of human androgen receptor complementary DNA and localization to the X chromosome. Science. 1988; 240:327–330. [PubMed: 3353727]

Miyamoto H, Rahman MM, Chang C. Molecular basis for the antiandrogen withdrawal syndrome. J Cell Biochem. 2004; 91:3–12. [PubMed: 14689576]

Murshudov GN, Vagin AA, Dodson EJ. Refinement of macromolecular structures by the maximum-likelihood method. Acta Crystallogr D Biol Crystallogr. 1997; 53:240–255. [PubMed: 15299926]

Navaza J. AMoRe: an automated package for molecular replacement. Acta Cryst A. 1994; A50:157–163.

Nishimura K, Ting HJ, Harada Y, Tokizane T, Nonomura N, Kang HY, Chang HC, Yeh S, Miyamoto H, Shin M, Aozasa K, Okuyama A, Chang C. Modulation of androgen receptor transactivation by gelsolin: a newly identified androgen receptor coregulator. Cancer Res. 2003; 63:4888–4894. [PubMed: 12941811]

Perrakis A, Morris R, Lamzin VS. Automated protein model building combined with iterative structure refinement. Nature structural biology. 1999; 6:458–463.

Quayle SN, Mawji NR, Wang J, Sadar MD. Androgen receptor decoy molecules block the growth of prostate cancer. Proc Natl Acad Sci U S A. 2007; 104:1331–1336. [PubMed: 17227854]

Ravindranathan P, Lee TK, Yang L, Centenera MM, Butler L, Tilley WD, Hsieh JT, Ahn JM, Raj GV. Peptidomimetic targeting of critical androgen receptor-coregulator interactions in prostate cancer. Nat Commun. 2013; 4:1923. [PubMed: 23715282]

Saha D, Banerjee S, Bashir S, Vijayraghavan U. Context dependent splicing functions of Bud31/Ycr063w define its role in budding and cell cycle progression. Biochem Biophys Res Commun. 2012; 424:579–585. [PubMed: 22789856]

Schrodinger LLC. The PyMOL Molecular Graphics System, Version 0.99. 2010

Shatkina L, Mink S, Rogatsch H, Klocker H, Langer G, Nestl A, Cato AC. The cochaperone Bag-1L enhances androgen receptor action via interaction with the NH2-terminal region of the receptor. Mol Cell Biol. 2003; 23:7189–7197. [PubMed: 14517289]

Shibata Y, Morita T, Kashiwagi B, Tomizawa H, Yamanaka H. Estramustine phosphate withdrawal syndrome with dramatic pain relief. J Urol. 1999; 162:805. [PubMed: 10458378]

Shyr CR, Tsai MY, Yeh S, Kang HY, Chang YC, Wong PL, Huang CC, Huang KE, Chang C. Tumor suppressor PAX6 functions as androgen receptor co-repressor to inhibit prostate cancer growth. Prostate. 2010; 70:190–199. [PubMed: 19790232]

Small EJ, Carroll PR. Prostate-specific antigen decline after casodex withdrawal: evidence for an antiandrogen withdrawal syndrome. Urology. 1994; 43:408–410. [PubMed: 7510915]

Trapman J, Dubbink HJ. The role of cofactors in sex steroid action. Best Pract Res Clin Endocrinol Metab. 2007; 21:403–414. [PubMed: 17875488]

van de Wijngaart DJ, Dubbink HJ, Molier M, de Vos C, Jenster G, Trapman J. Inhibition of androgen receptor functions by gelsolin FxxFF peptide delivered by transfection, cell-penetrating peptides, and lentiviral infection. Prostate. 2011; 71:241–253. [PubMed: 20690138]

van de Wijngaart DJ, van Royen ME, Hersmus R, Pike AC, Houtsmuller AB, Jenster G, Trapman J, Dubbink HJ. Novel FXXFF and FXXMF motifs in androgen receptor cofactors mediate high affinity and specific interactions with the ligand-binding domain. J Biol Chem. 2006; 281:19407–19416. [PubMed: 16690616]

Warnmark A, Treuter E, Gustafsson JA, Hubbard RE, Brzozowski AM, Pike AC. Interaction of transcriptional intermediary factor 2 nuclear receptor box peptides with the coactivator binding site of estrogen receptor alpha. J Biol Chem. 2002; 277:21862–21868. [PubMed: 11937504]

Watson PA, Chen YF, Balbas MD, Wongvipat J, Socci ND, Viale A, Kim K, Sawyers CL. Constitutively active androgen receptor splice variants expressed in castration-resistant prostate cancer require full-length androgen receptor. Proc Natl Acad Sci U S A. 2010; 107:16759–16765. [PubMed: 20823238]

Yang Z, Chang YJ, Yu IC, Yeh S, Wu CC, Miyamoto H, Merry DE, Sobue G, Chen LM, Chang SS, Chang C. ASC-J9 ameliorates spinal and bulbar muscular atrophy phenotype via degradation of androgen receptor. Nat Med. 2007; 13:348–353. [PubMed: 17334372]

Yeh S, Chang C. Cloning and characterization of a specific coactivator, ARA70, for the androgen receptor in human prostate cells. Proc Natl Acad Sci U S A. 1996; 93:5517–5521. [PubMed: 8643607]

Otwinowski Z, Minor W. Processing of X-ray Diffraction Data Collected in Oscillation Mode. Macromolecular Crystallography, part A. 1997; 276:307–326.

Highlights

- Anti-androgens-mutant-ARs had similar binary structure to the DHT-wild type-AR.

- These ARs bound to similar peptides with Fxx(F/H/L/W/Y)Y motifs.

- BUD31 with FxxFY motif was a new AR coregulator.

- BUD31-related peptides could suppress AR related function.

- Combined peptide screening and structure analysis for anti-ARs was proposed.
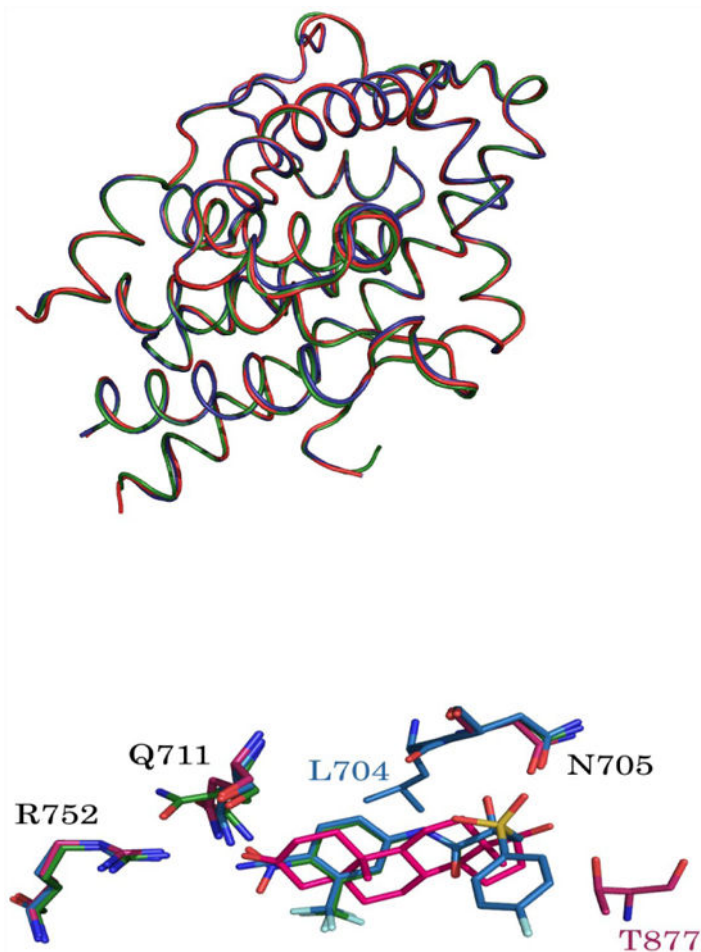
Fig. 1.
A. Superposition of the overall structures of WT- (red), T877A- (green), and W741L (blue)-AR-LBD. The overall structures of the WT-, T877A-, and W741L-AR-LBD are drawn with thin ribbon.

B. Overlapped crucial residues of active site in WT-, T877A-, and W741L-AR-LBD. Residues are shown with sticks. The DHY, HFT, and R-bic are illustrated as red, green, and blue. The fluorine, nitrogen oxygen, and phosphrous atoms are depicted as light green, blue, red, orange, respectively.
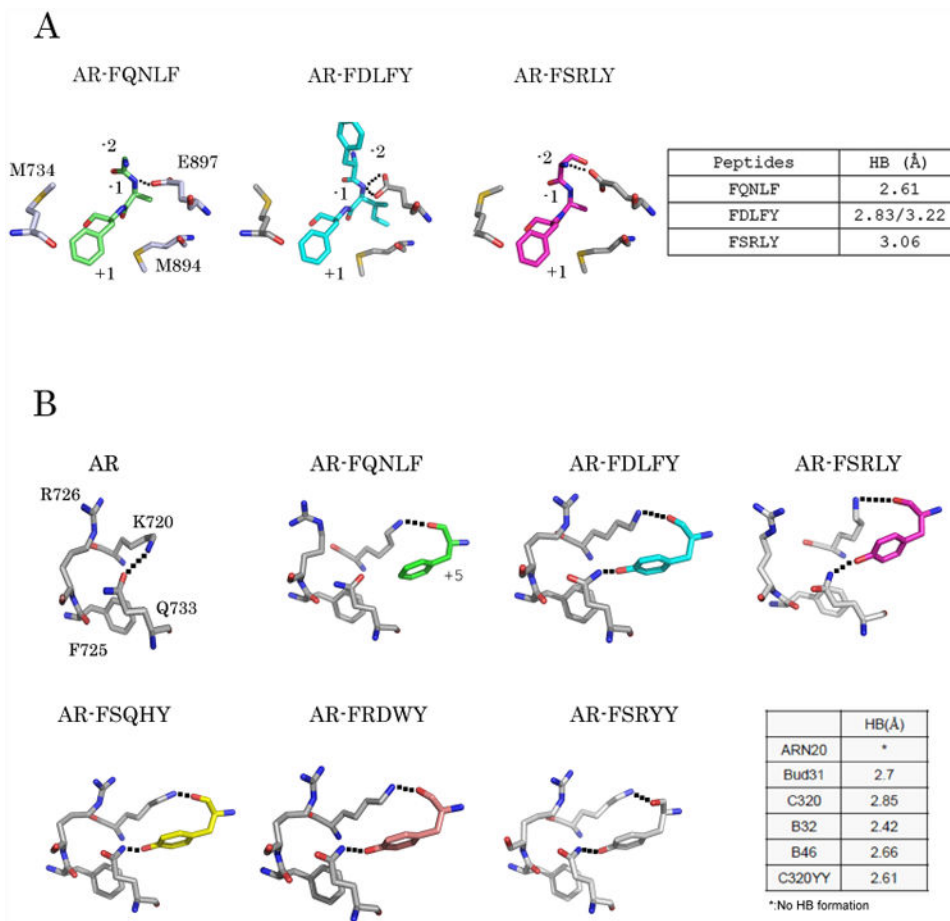
Fig. 2. Interactions in the AF2 site

Interactions between the peptides and proteins in front-end (A) and back-end (B) areas. Peptides are color-coded as follow: unbound, gray; FQNLF, green, FDLFY, cyan; FSRLY, magenta; FSQHY, yellow, and FSRYY, wheat. Residues are shown as sticks; carbon, nitrogen, and oxygen atoms are shown in gray, blue, and red, respectively. Hydrogen bond contacts are illustrated with black dashed lines. The lengths of the hydrogen bonds are summarized in the tables.
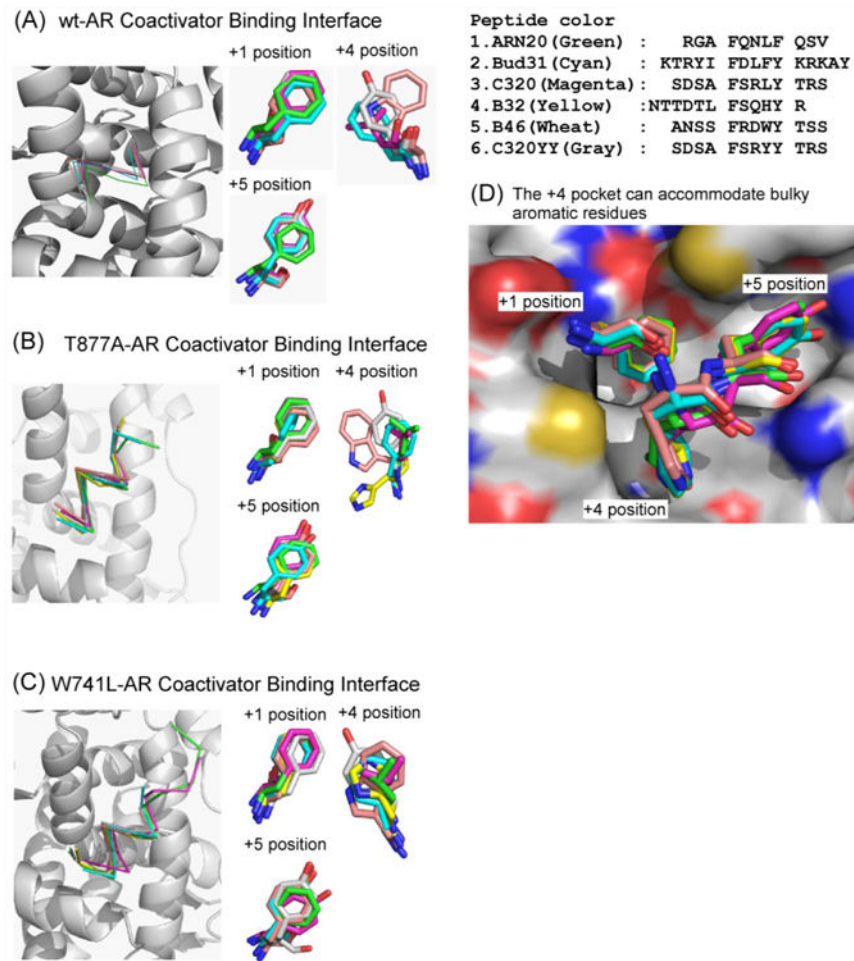
Fig. 3.
Interfaces between peptides and ARs.
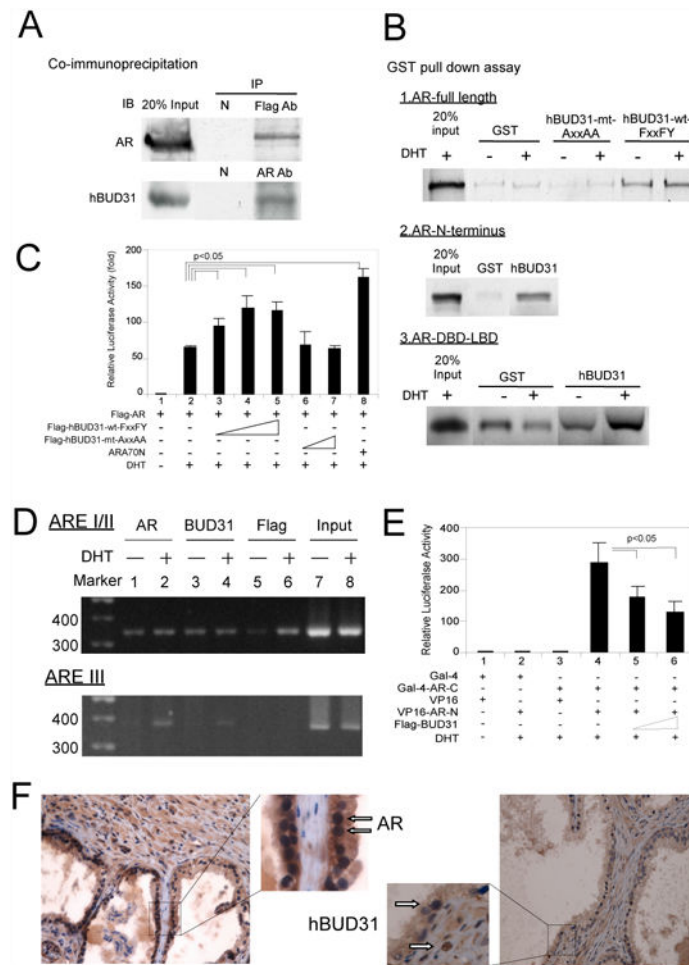
Fig. 4. Interaction between AR and BUD31

(A) Co-IP of Flag-BUD31 with endogenous AR in the prostate cancer cell line LNCaP. Extracts of LNCaP cells overexpressing 3xFlag-BUD31 were treated with 1 μM DHT. IP was performed using an anti-AR (C19) or anti-Flag antibody, or normal rabbit serum (negative control), followed by immunoblotting (IB) with antibodies to AR or BUD3. (B) BUD31 interacted with full-length AR and N- and C-terminal regions of the AR in GST pull-down assays; mutation of the FxxFY motif to AxxAA in BUD31 reduced BUD31 interactions with the AR. BUD31 enhanced AR transactivation and blocked AR N-C interactions. (C) PC-3 prostate cancer cells transfected with BUD31. PC-3 cells in 24-well plates were co-transfected with 300 ng of MMTV-LUC reporter plasmid and 0.5 ng of SV40-*Renilla* luciferase plasmid together with 100 ng of pCMV-Flag-AR, 100–500 ng of p3xFLAG-BUD31-wt-FxxFY or 100–500 ng p3xFLAG-BUD31-mt-AxxAA; plasmid DNA was brought to a total of 1 μg with pCMV. After 16 h, ethanol or 10 nM DHT was added and cells were incubated for an additional 16 h. Relative LUC activity was determined using the dual luciferase system. ARA70 served as a positive control. (D) BUD31 interacts with AR in promoter regions of target genes. LNCaP cells were transfected with P3xflag-BUD31 plasmid and cultured overnight. Soluble chromatin was prepared from LNCaP cells treated with or without DHT, and ChIP assays were performed using an antibody to AR (AR),

BUD31 (BUD31), Flag (Flag), and RNA polymerase II. The final DNA extracts were amplified using the primers for ARE I/II and ARE III, described in Materials and methods. (E) BUD31 blocked AR N-C interactions. PC-3 cells in 24-well plates were transfected with 200 ng of pG5-LUC reporter plasmid and 0.5 ng of SV40-*Renilla* luciferase plasmid together with various combinations of 200 ng of Gal-4-AR-C (amino acids 1–501), 200 ng of VP16-AR-N (amino acids 556–919), 200–400 ng of p3xFLAG-BUD31, as indicated; pCMV was added as necessary to bring the total to 1 μg plasmid DNA. After 16 h, ethanol or 10 nM DHT was added and cells were incubated for an additional 16 h. Luciferase activity was assessed using a dual luciferase assay system. (F) BUD31 is expressed in benign prostatic hyperplasia tissue. Human prostate gland tissues were immunostained for AR and BUD31. The arrows indicate ARs (left panel) and BUD31 (right panel). The figures are representative of three benign prostatic gland hyperplasia tissues.
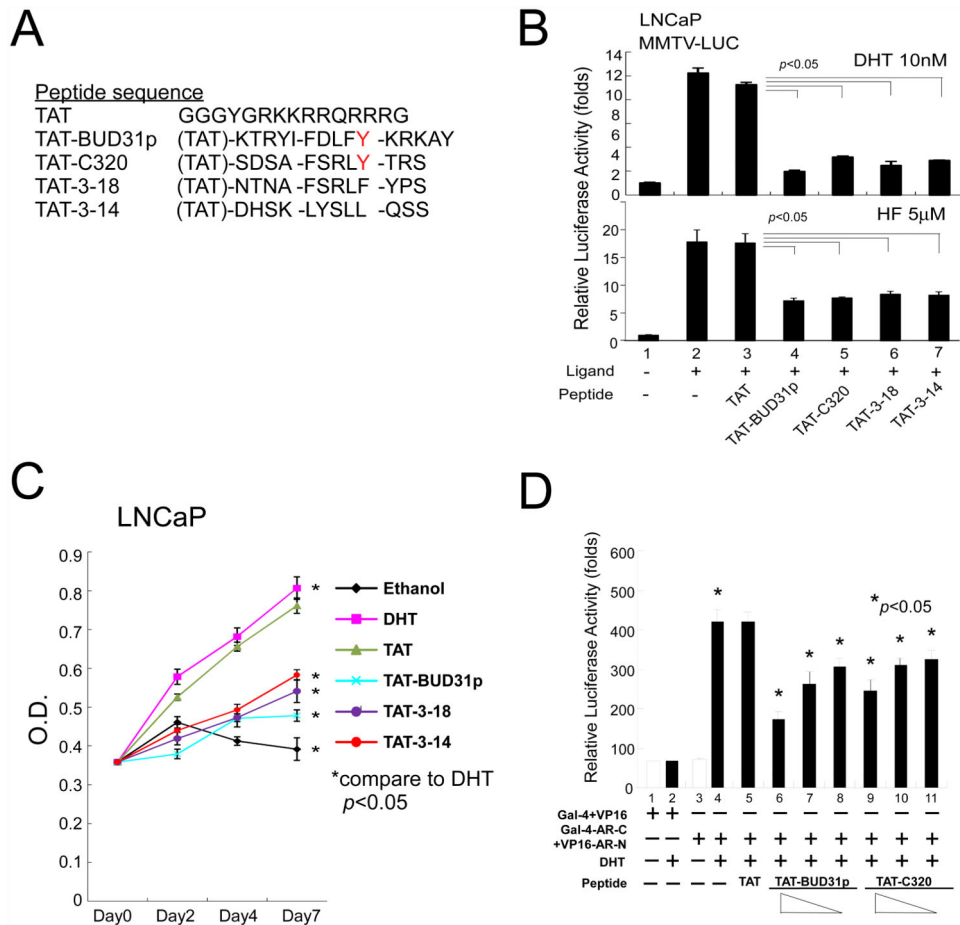
Fig. 5. BUD31 peptide potently suppresses AR-mediated function and growth of AR-harboring prostate cancer cells, and blocks AR N-C interactions

Short peptides of wt-BUD31, C320 (FxxLY motif), 3–18 (FxxLF motif) (Hsu et al., 2003), and 3-14 (LxxLL motif) peptides conjugated with TAT were synthesized and tested in LNCaP cells (B and C) and PC-3 cells (D) in the presence and absence of 0.2 nM DHT. (A) Peptide sequences. (B-D) Test peptides suppress AR transactivation in the presence of DHT or HF (B), suppress LNCaP cell growth *in vitro* (C), and block AR N-C interactions (D).

Table 1

Liganded-AR-DBD-LBD associated peptides

		-1	+1 +4+5	+6	wt-AR		T877A-AR		
					Ethanol	DHT	Ethanol	DHT	HF
Gal-4					1	1	1	1	1
1.	B310	SPTPH	FTRLF	HY	8	17810	60	12100	6717
2.	B426	EASNSS	FARLF	H	2	13500	10	9552	1513
3.	C317	TEPPAA	FRQLF	F	5	6600	15	5227	4380
4.	C314	SS	FADLW	RNEAT	7	1142	16	859	121
5.	B49	SK	FSQLY	SYEPP	12	1788	24	1032	318
6.	B423	SPTRL	FDHLY	MT	10	1216	20	401	168
7.	C33	ST	FESLY	NNMTA	20	1328	15	1018	399
8.	C320	SDSA	FSRLY	TRS	8	13365	20	12725	4650
9.	A41	SSGG	FERFY	IAQ	13	4314	21	3065	3510
10.	A48	DPPTSK	FSTFY	Q	8	32	13	12	18
11.	A49	VLPGST	FERFY	R	8	25	11	26	19
12.	B37	HNTK	FSTFY	NMD	12	9162	29	6245	8711
13.	B45	NTPL	FQTFY	NQR	15	18010	90	12560	17240
14.	C41	S	FYDFY	NGASTP	15	23	14	23	17
15.	B32	NTTDTL	FSQHY	R	10	41	11	32	25
16.	B34	SP	FEEHY	LSTQS	13	42	15	37	28
17.	B411	HPARTS	FETHY	M	13	13	9	13	16
18.	HF-26	HASP	FEMHY	LLG	12	8905	27	8401	8904
19.	B46	ANSS	FRDWY	TSS	10	792	14	376	1262
20.	A47	DSQYSS	FSRYY	K	11	21	10	19	15
21.	A310	SHSS	FYQYY	LDN	16	4771	28	3586	4461
22.	B311	HKASP	FNYYY	LN	22	46	23	33	38
23.	B414	NPRTPTT	FERYY		12	18	13	15	15
24.	A43	PAPK	FKEFF	YAE	4	8845	5	7352	8304

	-1	+1 +4+5	+6	wt-AR		T877A-AR		
				Ethanol	DHT	Ethanol	DHT	HF
25. HF-15	HTSM	FESFF	RKE	6	11500	20	13854	14523
*CON-1	MYKP	HNHHQ	TSS	1	2	2	4	5
**#3-18	NTNA	FSRLF	YPS	2	12530	9	10985	3890
***ARN20	RGA	FQNLF	QSV	3	1310	4	1578	1423
$D30	HPTHSSR	LWELL	MEATPTM	18	19860	415	18060	8803
$$BUD31	KTRYI	FDLFY	KRKAY	2	8945	4	11965	4870

*CON-1: negative control

**#3-18, ***ARN20, and $D30: positive controls

$$BUD31: fragment of novel AR coregulator candidate

Table 2

Comparisons of the kinetic constants for the interactions between the ARs and peptides.

Peptide	k_a (1/Ms)	k_d (1/s)	K_a (1/M)	K_d (M)
ARN20-wt	5.7E+04	3.0E-03	1.9E+07	5.3E-08
ARN20-LY	2.8E+04	2.9E-03	9.8E+06	1.0E-07
ARN20-FY	1.7E+05	6.5E-03	2.6E+07	3.8E-08
ARN20-HY	3.7E+01	5.1E-03	7.3E+03	1.4E-04
ARN20-WY	7.3E+03	3.6E-03	2.0E+06	5.0E-07
ARN20-YY	9.3E+03	8.2E-03	1.1E+06	8.8E-07
Peptide	k_a (1/Ms)	k_d (1/s)	K_a (1/M)	K_d (M)
C320-LY	2.0E+5	5.9E-3	3.4E+7	3.0E-8
C320-LF	5.9E+4	4.6E-3	1.3E+7	7.8E-8
C320-FY	1.2E+5	6.0E-3	1.9E+7	5.2E-8
C320-HY	1.4E+2	5.3E-3	2.6E+4	3.8E-5
C320-WY	4.7E+4	6.5E-3	7.2E+6	1.4E-7
C320-YY	9.7E+2	3.7E-3	2.6E+5	3.8E-6